

Possible Kitaev Quantum Spin Liquid State in 2D Materials with $S = 3/2$ Changsong Xu^{1,*}, Junsheng Feng^{2,3,*}, Mitsuaki Kawamura⁴, Youhei Yamaji⁵, Yousra Nahas¹, Sergei Prokhorenko¹, Yang Qi^{2,6,†}, Hongjun Xiang^{2,6,‡} and L. Bellaïche¹¹Physics Department and Institute for Nanoscience and Engineering, University of Arkansas, Fayetteville, Arkansas 72701, USA²Key Laboratory of Computational Physical Sciences (Ministry of Education), State Key Laboratory of Surface Physics, and Department of Physics, Fudan University, Shanghai 200433, People's Republic of China³School of Physics and Materials Engineering, Hefei Normal University, Hefei 230601, People's Republic of China⁴The Institute for Solid State Physics, The University of Tokyo, Kashiwa-shi, Chiba 277-8581, Japan⁵Department of Applied Physics, University of Tokyo, Hongo, Bunkyo-ku, Tokyo 113-8656, Japan⁶Collaborative Innovation Center of Advanced Microstructures, Nanjing 210093, People's Republic of China

(Received 12 December 2019; accepted 7 February 2020; published 27 February 2020)

Quantum spin liquids (QSLs) form an extremely unusual magnetic state in which the spins are highly correlated and fluctuate coherently down to the lowest temperatures, but without symmetry breaking and without the formation of any static long-range-ordered magnetism. Such intriguing phenomena are not only of great fundamental relevance in themselves, but also hold promise for quantum computing and quantum information. Among different types of QSLs, the exactly solvable Kitaev model is attracting much attention, with most proposed candidate materials, e.g., RuCl_3 and Na_2IrO_3 , having an effective $S = 1/2$ spin value. Here, via extensive first-principles-based simulations, we report the investigation of the Kitaev physics and possible Kitaev QSL state in epitaxially strained Cr-based monolayers, such as CrSiTe_3 , that rather possess a $S = 3/2$ spin value. Our study thus extends the playground of Kitaev physics and QSLs to $3d$ transition metal compounds.

DOI: 10.1103/PhysRevLett.124.087205

Enormous efforts have been made to realize quantum spin liquids (QSLs) since the pioneering work of Anderson and Fazekas in the 1970s [1,2]. Models with typical ingredients, such as geometrical frustration and antiferromagnetism (AFM), have been extensively studied [3]. Recently, the two-dimensional (2D) Kitaev model defined on a honeycomb lattice has attracted much attention, since its ground state is exactly proved to be QSL with Majorana fermion excitations [4]. Later work by Jackeli and Khaliullin demonstrated that such a model can be realized in certain transition metal compounds with strong spin-orbit coupling (SOC) [5]. Measurements also observed proximate Kitaev QSL in candidate materials, such as $\alpha\text{-RuCl}_3$ [6–8] and $(\text{Na}_{1-x}\text{Li}_x)_2\text{IrO}_3$ [9,10], which all have a spin state of effective $S = 1/2$, as well as a layered structure with edge-sharing octahedra and strong SOC from $4d$ or $5d$ transition metals. However, to the best of our knowledge, unambiguous demonstration of the Kitaev QSL is still lacking and a zigzag ordered state tends to form in the aforementioned materials at very low temperatures. Possible reasons are that (i) the structure distorts away from ideal honeycomb lattice and (ii) the relative strengths of isotropic exchange coupling and Kitaev interaction play a role in the forming of ground states [11,12]. It is thus necessary to search for other candidates and/or find a way to tune magnetic interactions, in order to create QSL systems.

Recently, atomic layers made of CrI_3 and CrGeTe_3 have been synthesized and found to be ferromagnetic, which resulted in a major surge of researches dedicated to two-dimensional magnetism [13,14]. CrI_3 and CrGeTe_3 share similarities in their crystal structure with $\alpha\text{-RuCl}_3$ and Na_2IrO_3 ; i.e., they all have a honeycomb lattice and edge-sharing octahedra. On the other hand, CrI_3 and CrGeTe_3 have a higher spin state than $\alpha\text{-RuCl}_3$ and Na_2IrO_3 , namely, $S = 3/2$ vs $S = 1/2$. At first thought, the FM nature and large S value, as well as the light SOC associated with Cr, seemingly exclude CrI_3 and CrGeTe_3 from being Kitaev QSL candidates. However, one of our recent works [15] hints that these systems exhibit finite Kitaev interaction that arises from heavy ligands of I/Te and thus may in fact be promising to find QSL. As a matter of fact, it is important to know that (1) such previous work adopted the general matrix form of the Hamiltonian

$$\mathcal{H} = \frac{1}{2} \sum_{i,j} \mathbf{S}_i \cdot \mathcal{J}_{ij} \cdot \mathbf{S}_j + \sum_i \mathbf{S}_i \cdot \mathcal{A}_{ii} \cdot \mathbf{S}_i, \quad (1)$$

where the first sum runs over all nearest neighbors and the second sum runs over all single sites, and (2) the \mathcal{J}_X , \mathcal{J}_Y , and \mathcal{J}_Z matrices, respectively, have the following forms,

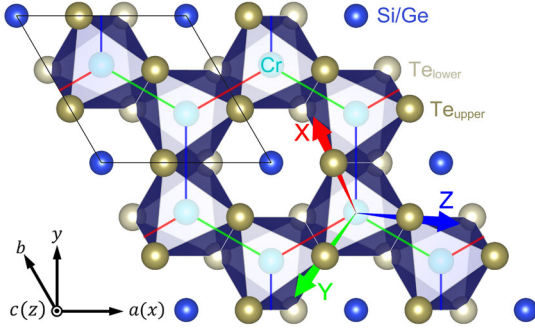


FIG. 1. Schematization of crystal structure and the Kitaev basis of CrSiTe_3 monolayer. The black parallelogram marks the unit cell of the honeycomb lattice of CrSiTe_3 monolayer. The $\{XYZ\}$ basis of the Kitaev model is indicated by red, green, and blue arrows, which is determined by Löwdin orthogonalization [17] of the hard axes of the nearest neighbor Cr-Cr interactions. The X, Y, and Z directions are found to be very close to the Cr-Te bonds [18].

$$\begin{pmatrix} J+K & \Gamma_2 & \Gamma_2 \\ \Gamma_2 & J & \Gamma_1 \\ \Gamma_2 & \Gamma_1 & J \end{pmatrix} \begin{pmatrix} J & \Gamma_2 & \Gamma_1 \\ \Gamma_2 & J+K & \Gamma_2 \\ \Gamma_1 & \Gamma_2 & J \end{pmatrix} \begin{pmatrix} J & \Gamma_1 & \Gamma_2 \\ \Gamma_1 & J & \Gamma_2 \\ \Gamma_2 & \Gamma_2 & J+K \end{pmatrix},$$

implying that Eq. (1) can be rewritten as

$$\mathcal{H} = \frac{1}{2} \sum_{i,j} \{ JS_i \cdot S_j + K S_i^\gamma S_j^\gamma + \Gamma_1 (S_i^\alpha S_j^\beta + S_i^\beta S_j^\alpha) + \Gamma_2 (S_i^\gamma S_j^\alpha + S_i^\alpha S_j^\gamma + S_i^\beta S_j^\gamma + S_i^\gamma S_j^\beta) \} + \sum_i A_{zz} S_i^z S_i^z, \quad (2)$$

where $\{\alpha, \beta, \gamma\} = \{Y, Z, X\}$, $\{Z, X, Y\}$, and $\{X, Y, Z\}$ for the X, Y, and Z bonds, respectively. Note that the global $\{XYZ\}$ basis and the X, Y, and Z bonds are shown in Fig. 1, and that only the A_{zz} component is finite in the \mathcal{A} matrix when expressed in the global $\{xyz\}$ basis—which explains why only A_{zz} appears in the single ion anisotropy (SIA) term. Interestingly, Eq. (2) characterizes a typical $JK\Gamma$ model [16] but with an extra SIA term. Consequently, Eq. (2) represents what we coin here as a $JK\Gamma A$ model.

Equations (1) and (2) have previously naturally reproduced and explained, in Ref. [15], the distinct magnetic behaviors of CrI_3 and CrGeTe_3 (that is, Ising vs Heisenberg behavior, respectively) [19,20]. The approach to induce Kitaev interaction by means of heavy ligands [15] is also evidenced by a subsequent work [21] that proposes achieving high-spin Kitaev physics in systems with strong SOC in anions and strong Hund's coupling in transition metal cations. Moreover, the non-negligible effects of Kitaev interaction have also been verified by magnetization measurements on CrBr_3 monolayer [22] and magnon experiments on CrI_3 monolayer [23]. It therefore appears legitimate to explore Kitaev QSL states in Cr-based monolayers (which would then be the first Kitaev QSL candidates with partially filled $3d$ electrons and $S = 3/2$),

provided there is a way to make the isotropic exchange coefficient J zero or nearly so while keeping K finite. The way we are going to pursue, in order to accomplish such annihilation, is to apply epitaxial strain, since it has been shown to be an effective approach to tune the strength of exchange couplings, and thus the Curie temperature, of Cr-based systems [24]. We chose here to study CrSiTe_3 (CST) and CrGeTe_3 (CGT) under compressive strain because, as we will see, their J coefficient is rather sensitive to such strain. CST has the same structure as CGT, and exhibits a similar Heisenberg behavior as CGT but with an additional slightly favoring out-of-plane anisotropy [25,26] [note that properties of CST, including the nature of its FM state, can be well explained by Eq (2) as well [15]].

Technically, the elements of the exchange matrix \mathcal{J} , as well as the SIA coefficient A_{zz} , are obtained by performing density functional theory (DFT) calculations, together with the four-state energy mapping method [15,27,28], for any investigated epitaxial strain in CST and CGT. These first-principles-derived magnetic parameters are then used as inputs of both classical Monte Carlo (MC) simulations and quantum simulations using a thermal pure quantum (TPQ) states method [29]. As we will show below, such simulations reveal the existence of a strain-driven intermediate state bridging FM and AFM phases in CST and CGT, with this bridging state possessing many hallmarks of QSL, that are a double peak in the specific heat vs temperature function and a low-temperature plateau in the temperature evolution of the entropy. This Letter particularly focuses on CST, while (qualitatively identical) results for CGT are reported in the Supplemental Material [30].

Figures 2(a) and 2(b) report the behaviors of the magnetic parameters of Eq. (2) as a function of compressive strain η in CST, as predicted by DFT. Specifically, the isotropic J parameter has a value of -3.42 meV at zero strain (relaxed case), which is indicative of the FM nature of CST. But then, J changes its sign at -2.41% and therefore favors an AFM state when further increasing the magnitude of the compressive strain. It is further found that another diagonal element of the \mathcal{J} matrices indicated above (i.e., $J + K$) changes its sign at -2.25% . On the other hand, the Kitaev coefficient K is 0.34 meV at zero strain and only slightly decreases when increasing the magnitude of strain η . In particular, K almost remains constant at 0.275 meV around the strain range between -2.25% and -2.41% . Furthermore, when increasing the magnitude of strain η , the SIA coefficient A_{zz} slightly increases and keeps the value of 0.22 meV between $\eta = -2\%$ and -4% . The opposite behaviors of K and A_{zz} upon varying strain, though weak, lead to the total anisotropy being in-plane when $\eta < -0.02$, since it is previously determined that the K term favors out-of-plane (through a frustration mechanism), while SIA favors in plane for CST [15]. Moreover, the other terms of the \mathcal{J} matrices, that are Γ_1 and Γ_2 , are found to be around an order smaller than K , and also change slowly with strain.

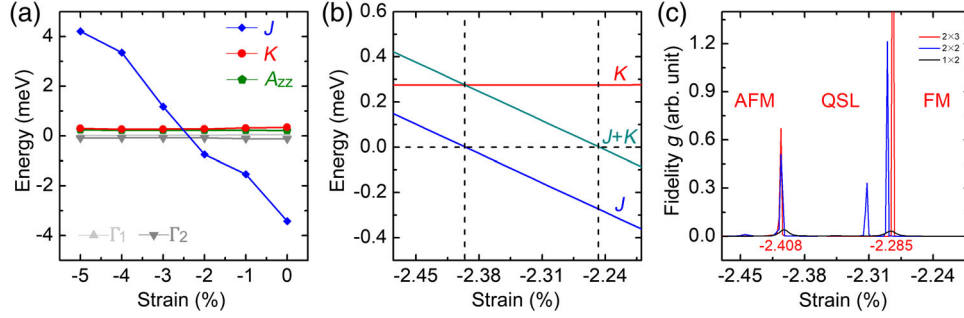


FIG. 2. Magnetic coefficients and fidelity of CrSiTe₃ monolayer. Panel (a) display the evolution of magnetic coefficients as a function of compressive strain. Panel (b) further shows the evolution of J , $J + K$, and K for a specific strain region. The horizontal dashed line indicates the zero in energy, while the vertical lines mark the critical strains at which J or $J + K$ becomes zero. Panel (c) shows the quantity of fidelity g as a function of strain for different sizes of supercells.

Interestingly and according to the Kitaev model [4], the vanishing of J (or $J + K$) and the large value of K hint toward the possibility of forming a QSL state near the boundary between FM and AFM states, as is in line with a recent study [41]. Additionally, in our model, there is also a finite SIA term, in the strain range where K is finite but J (or $J + K$) vanishes. The effect of such a SIA term to the existence of QSL is unknown, to the best of our knowledge.

To determine the phase diagram of CST in its stability region and search for possible QSL states, we now compute the quantity of fidelity using the exact diagonalization (ED) method. Practically, the DFT-extracted magnetic parameters at different strains are inserted into ED quantum simulations, from which the ground-state wave functions are obtained. The fidelity metric g , which measures changes in ground-state wave functions, is then calculated as [42]

$$g = \frac{2}{N_s} \frac{1 - F(\mu, \delta\mu)}{(\delta\mu)^2}, \quad (3)$$

where $F(\mu, \delta\mu) = |\langle \Psi(\mu) | \Psi(\mu + \delta\mu) \rangle|$ is the overlap between two ground-state wave functions at strain μ and $\mu + \delta\mu$ with $\delta\mu \rightarrow 0$, and N_s is the number of sites. As $F(\mu, \delta\mu)$ equals 0 for two states that are exactly orthogonal, a peak in fidelity g will be detected at the boundary of a phase transition; on the other hand, $F(\mu, \delta\mu)$ is nearly 1 for two states that are similar to each other and the fidelity g will then show no obvious changes in such a case. The fidelity is originally a concept of quantum information, but has been recently proven to be very successful in identifying quantum phase transitions, in particular in ED simulations with limited system sizes [43,44]. It can accurately predict phase transition on the premise that the supercell (and thus N_s) are large enough. For a small size of supercells, the scaling approach is commonly used: by increasing the size of supercells, the true peaks in fidelity g become sharper, while the “fake” ones should gradually vanish.

We thus calculated the fidelity g for 1×2 , 2×2 , and 2×3 supercells that contain 4, 8, and 12 sites, respectively. As shown in Fig. 2(c), in the strain range extending from

−2.20% to −2.47%, two groups of peaks are found to not only exist for all three supercells, but also become sharper with increasing size of supercells, with one group at $\eta \approx -2.4\%$ and the other group at $\eta \approx -2.29\%$. On the other hand, another peak at $\eta \approx -2.31\%$ only exists for the 2×2 supercell, and can thus be considered to be fake. It is therefore legitimate to conclude that, up to the sizes we studied, the two peaks for the 2×3 supercell correspond to phase transitions. The first peak is located at −2.285%, which is near the aforementioned −2.25%, at which ($J + K$) changes its sign, and the second one is determined to be at −2.408%, which is rather close to −2.41% for which J becomes zero.

The dipolar patterns resulting from corresponding *classical* MC simulations indicate that the phase at small strain is a FM state, as consistent with the observed FM state at zero strain [25,26], while the phase at the largest compressive strain is a Néel-type AFM state, as also consistent with recent calculations on compressive strained CrI₃ [45]. On the other hand, the magnetic dipoles obtained from classical MC computations in the stability region of the intermediate phase (between −2.25% and −2.41%) exhibit a more complex pattern. As we can see in Fig. 3(a), besides the FM domain, the zigzag AFM domains begin to emerge at the phase boundary of the FM state and the intermediate phase. As further shown in Fig. 3(d), both ferromagnetically coupled pairs and antiferromagnetically coupled pairs exist near the other phase boundary between the intermediate phase and AFM state. Such coexistence of FM and AFM indicates high frustration in the intermediate state. Moreover, vortices and antivortices made of magnetic dipoles appear at both phase boundaries and are found to bond to each other at $\eta = -2.25\%$, which reminds us about the Berezinskii-Kosterlitz-Thouless (BKT) phase [46,47]. Interestingly, the BKT phase is sometimes viewed as the classical analogue of QSL [12,48]. Furthermore, Figs. 3(b) and 3(c) show nearly degenerate low-energy spin patterns (among many others) within the intermediate phase.

Let us also compute two other quantities from quantum simulations that can provide signatures of QSL states,

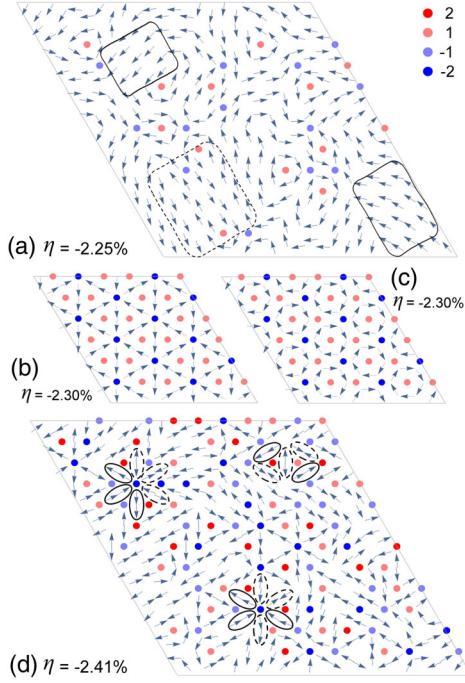


FIG. 3. Patterns of magnetic dipole moments at different strains in CrSiTe₃ monolayer. (a) Spin patterns at $\eta = -2.25\%$, at which $J + K$ changes its sign. The solid and dashed rectangle marks the FM and zigzag AFM domains, respectively. Vortices and antivortices are indicated by the red and blue dots, respectively. The values represented by the dots are the vortex number, which is defined as $n = (1/2\pi) \sum_{i=1}^6 \Delta\theta_i$, where the rotation from $i = 1-6$ is done in an anticlockwise fashion. (b),(c) Energetically degenerate states at $\eta = -2.30\%$. (d) Spin textures at $\eta = -2.41\%$, at which J changes its sign. The solid and dashed ellipses mark ferromagnetic and antiferromagnetic pairs, respectively. Note that our MC simulations are followed by a conjugate gradient algorithm, indicating that the spin patterns shown here are at global or local minima [31].

which are the specific heat C and the thermal entropy S . Practically, the temperature evolution of C and S are calculated in our systems using the TPQ method,

$$C = \frac{d\langle\phi_T|\hat{H}|\phi_T\rangle}{dT}, \quad (4)$$

$$S = Nk_B \ln 4 - \int_T^{+\infty} dT' \frac{C}{dT'}, \quad (5)$$

where ϕ_T is the TPQ state at T (see Ref. [12] for details). According to previously established theory, spin-1/2 Kitaev QSL should exhibit two peaks in the specific heat, with the one at higher (lower) temperature being associated with localized (itinerant) Majorana fermions [12,49,50]. Consequently, entropy release should occur twice when lowering temperature, between which a plateau should exist. For a pure higher-spin Kitaev model without further terms, Majorana fermions can be maintained [51] and the plateau is predicted to locate at $\frac{1}{2}Nk_B \ln(2S + 1)$ [52], while the effects of J , Γ , or SIA are yet to be determined, to the best of our knowledge. We thus decided to calculate the specific C and thermal entropy S for three specific strains, -2.20% , -2.34% , and -2.56% , corresponding to the different phase zones identified by the fidelity g . Results are shown in Fig. 4. For the smallest-in-magnitude strain of -2.20% , the specific heat C shows a single peak at $T = 6.3$ K, indicating a paramagnetic (PM) to FM transition there. The corresponding entropy S smoothly decreases to zero as the temperature decreases toward 0 K. Similarly, for the largest-in-magnitude strain of -2.56% , a single peak in C marks a PM to AFM transition at $T = 11.5$ K, and the temperature dependence of S is rather monotonic. Strikingly, for the intermediate strain at -2.34% , a double-peak structure is clearly identified in

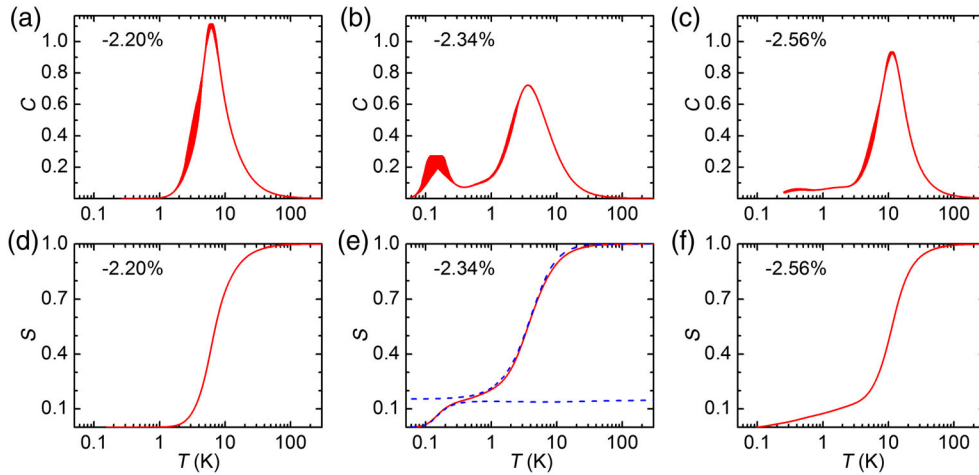


FIG. 4. Temperature evolution of specific heat and entropy of CrSiTe₃ monolayer at different strains. Panels (a)–(c) display the specific heat in units of meV K, while panels (d)–(f) show entropy in units of $Nk_B \ln 4$ as a function of temperature. The 2×3 honeycomb lattice is used with $N = 12$.

the specific heat C , with one at the higher temperature, $T_h = 3.7$ K, and one at the lower temperature, $T_l = 0.15$ K. Such a double-peak structure, corresponding to Majorana fermion excitations, strongly further supports the existence of Kitaev QSL around strain of -2.34% . Moreover, as previously reported, the ratio between T_l and T_h can be a quantitative measure for the distance to Kitaev QSL, as $T_l/T_h = 0.03$ for typical Kitaev QSL and $T_l/T_h = 0.11$ for Na_2IrO_3 [12]. Here, at strain of -2.34% , the T_l/T_h ratio is determined to be 0.04, which further emphasizes a state rather close to Kitaev QSL. For the strain of -2.34% , the entropy shows a clear plateau at 0.154 in units of $Nk_B \ln 4$, which is different from the 0.5 value of the pure Kitaev model [52], but which is in line with the remarkably lowered value of 0.1935 in the presence of the Γ_1 term [53]. As mentioned previously, the distinct double peak in C and the plateau in entropy further strongly suggest that the predicted intermediate phase is indeed a Kitaev QSL.

To conclude, we have combined DFT calculations, classical MC computations, and quantum simulations to predict a possible strain-induced Kitaev QSL state in epitaxial CrSiTe_3 and CrGeTe_3 monolayers. Such $3d$ transition metal compounds, together with strain engineering allowing to continuously tune the J/K ratio, largely expand the scope of candidates to realize Kitaev QSL.

We thank Dr. Ziyang Meng and Dr. Zhengxin Liu for useful discussion. This work is partly supported by the Department of Energy, Office of Basic Energy Sciences, under Award No. DE-SC0002220 (results for Figs. 2(a) and 2(b)) and partly by the Arkansas Research Alliance (other results). DARPA Grant No. HR0011727183-D18AP00010 (TEE Program) is also acknowledged for the investigation of topological aspects. J.F. acknowledges the support from Anhui Provincial Natural Science Foundation (1908085MA10). M.K. is supported by Priority Issue (creation of new functional devices and high-performance materials to support next-generation industries) to be tackled by using Post ‘K’ Computer from the MEXT of Japan. Y.Q. is supported by NSFC (11874115). H.X. is supported by NSFC (11825403), Program for Professor of Special Appointment (Eastern Scholar), Qing Nian Ba Jian Program, and Fok Ying Tung Education Foundation. The Arkansas High Performance Computing Center (AHPCC) is also acknowledged.

*These authors contributed equally to this work.

†qiyang@fudan.edu.cn

‡hxiang@fudan.edu.cn

- [1] P. W. Anderson, *Mater. Res. Bull.* **8**, 153 (1973).
 [2] P. Fazekas and P. W. Anderson, *Philos. Mag.* **30**, 423 (1974).
 [3] L. Balents, *Nature (London)* **464**, 199 (2010).
 [4] A. Kitaev, *Ann. Phys. (Amsterdam)* **321**, 2 (2006).

- [5] G. Jackeli and G. Khaliullin, *Phys. Rev. Lett.* **102**, 017205 (2009).
 [6] A. Banerjee, C. Bridges, J.-Q. Yan, A. Aczel, L. Li, M. Stone, G. Granroth, M. Lumsden, Y. Yiu, J. Knolle *et al.*, *Nat. Mater.* **15**, 733 (2016).
 [7] S.-H. Baek, S.-H. Do, K.-Y. Choi, Y. S. Kwon, A. U. B. Wolter, S. Nishimoto, J. van den Brink, and B. Büchner, *Phys. Rev. Lett.* **119**, 037201 (2017).
 [8] J. Zheng, K. Ran, T. Li, J. Wang, P. Wang, B. Liu, Z.-X. Liu, B. Normand, J. Wen, and W. Yu, *Phys. Rev. Lett.* **119**, 227208 (2017).
 [9] G. Cao, T. F. Qi, L. Li, J. Terzic, V. S. Cao, S. J. Yuan, M. Tovar, G. Murthy, and R. K. Kaul, *Phys. Rev. B* **88**, 220414(R) (2013).
 [10] S. Manni, S. Choi, I. I. Mazin, R. Coldea, M. Altmeyer, H. O. Jeschke, R. Valentí, and P. Gegenwart, *Phys. Rev. B* **89**, 245113 (2014).
 [11] J. Chaloupka, G. Jackeli, and G. Khaliullin, *Phys. Rev. Lett.* **110**, 097204 (2013).
 [12] Y. Yamaji, T. Suzuki, T. Yamada, S.-i. Suga, N. Kawashima, and M. Imada, *Phys. Rev. B* **93**, 174425 (2016).
 [13] B. Huang, G. Clark, E. Navarro-Moratalla, D. R. Klein, R. Cheng, K. L. Seyler, D. Zhong, E. Schmidgall, M. A. McGuire, D. H. Cobden *et al.*, *Nature (London)* **546**, 270 (2017).
 [14] C. Gong, L. Li, Z. Li, H. Ji, A. Stern, Y. Xia, T. Cao, W. Bao, C. Wang, Y. Wang *et al.*, *Nature (London)* **546**, 265 (2017).
 [15] C. Xu, J. Feng, H. Xiang, and L. Bellaïche, *npj Comput. Mater.* **4**, 57 (2018).
 [16] S. M. Winter, A. A. Tsirlin, M. Daghofer, J. van den Brink, Y. Singh, P. Gegenwart, and R. Valenti, *J. Phys. Condens. Matter* **29**, 493002 (2017).
 [17] P.-O. Löwdin, *J. Chem. Phys.* **19**, 1396 (1951).
 [18] The X , Y , and Z directions also correspond to the unique direction associated with the $J + K$ diagonal element of the \mathcal{J} matrix indicated above Eq. (2) for the X (red), Y (green), and Z (blue) Cr—Cr bonds, respectively. Note that italic fonts X , Y , and Z are used for axes vs roman fonts X , Y , or Z for bonds.
 [19] N. Samarth, *Nature (London)* **546**, 216 (2017).
 [20] J. L. Miller, *Phys. Today* **70**, No. 7, 16 (2017).
 [21] P. P. Stavropoulos, D. Pereira, and H.-Y. Kee, *Phys. Rev. Lett.* **123**, 037203 (2019).
 [22] M. Kim, P. Kumaravel, J. Birkbeck, W. Kuang, S. Xu, D. Hopkinson, J. Knolle, P. McClarty, A. Berdyugin, M. B. Shalom *et al.*, *National electronics review* **2**, 457 (2019).
 [23] I. Lee, F. G. Utermohlen, D. Weber, K. Hwang, C. Zhang, J. van Tol, J. E. Goldberger, N. Trivedi, and P. C. Hammel, *Phys. Rev. Lett.* **124**, 017201 (2020).
 [24] X. Li and J. Yang, *J. Mater. Chem. C* **2**, 7071 (2014).
 [25] V. Carreau, F. Moussa, and M. Spiesser, *Europhys. Lett.* **29**, 251 (1995).
 [26] T. J. Williams, A. A. Aczel, M. D. Lumsden, S. E. Nagler, M. B. Stone, J.-Q. Yan, and D. Mandrus, *Phys. Rev. B* **92**, 144404 (2015).
 [27] H. Xiang, C. Lee, H.-J. Koo, X. Gong, and M.-H. Whangbo, *Dalton Trans.* **42**, 823 (2013).
 [28] C. Xu, B. Xu, B. Dupé, and L. Bellaïche, *Phys. Rev. B* **99**, 104420 (2019).

- [29] S. Sugiura and A. Shimizu, *Phys. Rev. Lett.* **108**, 240401 (2012).
- [30] See Supplemental Material at <http://link.aps.org/supplemental/10.1103/PhysRevLett.124.087205> for detailed methods and further discussions, which includes Refs. [15,17,27–29,31–40].
- [31] C. Xu, Y. Nahas, S. Prokhorenko, J. Feng, H. Xiang, and L. Bellaiche, *Phys. Rev. B* **101**, 060404(R) (2020).
- [32] G. Kresse and D. Joubert, *Phys. Rev. B* **59**, 1758 (1999).
- [33] P. E. Blöchl, *Phys. Rev. B* **50**, 17953 (1994).
- [34] Y. Miyatake, M. Yamamoto, J. Kim, M. Toyonaga, and O. Nagai, *J. Phys. C* **19**, 2539 (1986).
- [35] M. R. Hestenes and E. Stiefel, *Methods of Conjugate Gradients for Solving Linear Systems* (National Bureau of Standards, Washington, DC, 1952), Vol. 49.
- [36] M. Kawamura, K. Yoshimi, T. Misawa, Y. Yamaji, S. Todo, and N. Kawashima, *Comput. Phys. Commun.* **217**, 180 (2017).
- [37] A. V. Knyazev, *SIAM J. Sci. Comput.* **23**, 517 (2001).
- [38] M. McGuire, *Crystals* **7**, 121 (2017).
- [39] Y. S. Hou, H. J. Xiang, and X. G. Gong, *Phys. Rev. B* **96**, 054410 (2017).
- [40] L. Clark, G. Sala, D. D. Maharaj, M. B. Stone, K. S. Knight, M. T. Telling, X. Wang, X. Xu, J. Kim, Y. Li *et al.*, *Nat. Phys.* **15**, 262 (2019).
- [41] S. H. Chun, J.-W. Kim, J. Kim, H. Zheng, C. C. Stoumpos, C. Malliakas, J. Mitchell, K. Mehlawat, Y. Singh, Y. Choi *et al.*, *Nat. Phys.* **11**, 462 (2015).
- [42] S. Yang, K. Sun, and S. Das Sarma, *Phys. Rev. B* **85**, 205124 (2012).
- [43] H. T. Quan, Z. Song, X. F. Liu, P. Zanardi, and C.-P. Sun, *Phys. Rev. Lett.* **96**, 140604 (2006).
- [44] S.-J. Gu, *Int. J. Mod. Phys. B* **24**, 4371 (2010).
- [45] F. Zheng, J. Zhao, Z. Liu, M. Li, M. Zhou, S. Zhang, and P. Zhang, *Nanoscale* **10**, 14298 (2018).
- [46] V. Berezinsky, *Zh. Eksp. Teor. Fiz.* **61**, 1144 (1972) [*Sov. Phys. JETP* **34**, 610 (1972)].
- [47] J. M. Kosterlitz and D. J. Thouless, *J. Phys. C* **6**, 1181 (1973).
- [48] C. C. Price and N. B. Perkins, *Phys. Rev. Lett.* **109**, 187201 (2012).
- [49] G. Baskaran, S. Mandal, and R. Shankar, *Phys. Rev. Lett.* **98**, 247201 (2007).
- [50] J. Nasu, M. Udagawa, and Y. Motome, *Phys. Rev. B* **92**, 115122 (2015).
- [51] G. Baskaran, D. Sen, and R. Shankar, *Phys. Rev. B* **78**, 115116 (2008).
- [52] J. Oitmaa, A. Koga, and R. R. P. Singh, *Phys. Rev. B* **98**, 214404 (2018).
- [53] A. Catuneanu, Y. Yamaji, G. Wachtel, Y. B. Kim, and H.-Y. Kee, *npj Quantum Mater.* **3**, 23 (2018).